Chinese Chemical Letters 34 (2023) 108200

Contents lists available at ScienceDirect

Chinese Chemical Letters

journal homepage: www.elsevier.com/locate/cclet

A biologically stable, self-catalytic DNAzyme machine encapsulated by metal-phenolic nanoshells for multiple microRNA imaging

Xin Jin[a,1], Qin Wang[a,b,1], Jiezhou Pan[a], Jin Wang[a], Yunxiang He[a,e], Jiaojiao Shang[a,e], Mei Chen[a], Xianglian He[a], Yaoyao Zhang[f], Bo Wang[g], Yajie Wang[h], Guidong Gong[a,e,*], Junling Guo[a,c,d,e,*]

[a] BMI Center for Biomass Materials and Nanointerfaces, College of Biomass Science and Engineering, Sichuan University, Chengdu 610065, China
[b] School of Pharmacy, Southwest Minzu University, Chengdu 610225, China
[c] Department of Chemical and Biological Engineering, Bioproducts Institute, University of British Columbia, Vancouver BC V6T 1Z4, Canada
[d] State Key Laboratory of Polymer Materials Engineering, Sichuan University, Chengdu 610065, China
[e] National Engineering Laboratory for Clean Technology of Leather Manufacture, Sichuan University, Chengdu 610065, China
[f] Department of Obstetrics and Gynecology, Key Laboratory of Birth Defects and Related of Women and Children of Ministry of Education, The Reproductive Medical Center, West China Second University Hospital, Sichuan University, Chengdu 610041, China
[g] CAS Key Laboratory of Quantitative Engineering Biology, Shenzhen Institute of Synthetic Biology, Shenzhen Institutes of Advanced Technology, Chinese Academy of Sciences, Shenzhen 518055, China
[h] School of Engineering, Westlake University, Hangzhou 310034, China

ARTICLE INFO

Article history:
Received 20 September 2022
Revised 3 February 2023
Accepted 8 February 2023
Available online 16 February 2023

Keywords:
DNAzyme machine
Metal-phenolic nanoshells
Interference protection
Cofactors self-supply
Cell imaging

ABSTRACT

DNAzyme machines play critical roles in the fields of cell imaging, disease diagnosis, and cancer therapy. However, the applications of DNAzyme machines are limited by the nucleases-induced degradation, non-specific binding of proteins, and insufficient provision of cofactors. Herein, protected DNAzyme machines with different cofactor designs (referred to as ProDs) were nanoengineered by the construction of multifunctional metal-phenolic nanoshells to deactivate the interferential proteins, including nucleases and non-specific binding proteins. Moreover, the nanoshells not only facilitate the cellular internalization of ProDs but provide specific metal ions acting as cofactors of the designed DNAzymes. Cellular imaging results demonstrated that ProDs could effectively and simultaneously monitor multiple tumor-related microRNAs in living cells. This facile and rapid strategy that encapsulates DNAzyme machines into the protective metal-phenolic nanoshells is anticipated to extend to a wide range of functional nucleic acids-based biomedical applications.

Functional nucleic acids (FNAs) have been shown as a versatile platform owing to the sensitive molecular recognition capabilities based on the base-pairing principle and the affinity interaction [1–6]. Materials derived from FNAs play critical roles in the fields of cell imaging [7–9], disease diagnosis [10–12], and cancer therapy [13–16]. RNA-cleaving DNA enzymes (DNAzymes) are a class of single-stranded DNA molecules with catalytic activities to cleavage specific sequences of RNA or DNA, with the use of metal ions as cofactors (*e.g.*, Mg^{2+}, Na^{+}, Zn^{2+}, Cu^{2+}) [17–22].

DNAzymes have been explored as biological probes for monitoring microRNAs (miRNAs) [23], metal ions [24,25], and ATP [26] in living cells. However, the exposed single-stranded DNA molecules are easily invalidated by nucleases or non-specific binding proteins [27–29]. Therefore, the strategy of optimizing the structure of DNAzymes has been explored [3,7,30–32]. For example, spherical nucleic acids (SNAs) including gold nanoparticle-based DNAzyme machines (Dzm-machines) show relatively stronger resistance to the nucleases-induced degradation (*e.g.*, deoxyribonuclease I, DNase I), because of the negatively charged surface of the nucleic acid-formed particles driving high local salt concentrations, which can partially inhibit the activity of nucleases [30,33–36]. Nevertheless, this strategy cannot fully inactivate the nucleases and avoid the non-specific binding of proteins (*e.g.*, single-stranded DNA-binding protein, SSB protein) to the Dzm-machines. Therefore, the encapsulation of Dzm-machines within nanostructured shells possessing extremely small meshes (~10 nm) has been developed to prevent the DNA-based probes from the interference

* Corresponding authors.
E-mail addresses: guidong-gong@qq.com (G. Gong), junling.guo@scu.edu.cn (J. Guo).
[1] These authors contributed equally to this work.

https://doi.org/10.1016/j.cclet.2023.108200
1001-8417/

of nucleases and non-specific proteins [37–39]. However, due to the exceedingly small size of the interferential proteins (*e.g.*, DNase I and SSB protein, ~5–7 nm) [32], the mesh-structured protection strategies simply based on size exclusion mechanism are synthetically challenging and complicated in order to construct nanoshells with ultra-small and uniform meshes [35,40–42]. Furthermore, the simultaneous detection of multiple miRNAs is pivotal to understanding pathological development due to the key regulatory roles of miRNAs in gene expression [43]. However, the limited variety and provision number of cofactors significantly hamper the development of multiple miRNA recognition nanosystems. Therefore, a versatile and integral system is urgently needed to systematically improve the stability of the Dzm-machines in the complex biological environment and achieve sufficient multiple cofactors provision in living cells.

Herein, we show that Dzm-machines can be encapsulated individually by biocompatible supramolecular nanoshells composed of tannic acids (TA) and specific metal ions corresponding to different designs of cofactors, including Zn^{II}-incorporated Dzm_{Zn}-machines ($ProD_{Zn}$), Cu^{II}-incorporated Dzm_{Cu}-machines ($ProD_{Cu}$), and Zn^{II}/Cu^{II}-incorporated $Dzm_{Zn/Cu}$-machines ($ProD_{Zn/Cu}$) (Fig. S1 in Supporting information). The constructive building blocks for this nanoshell are mainly abundant plant extracts and already have been used as functional materials in advanced therapies and cell engineering [44–50], due to their high biocompatibility, versatile functionalization, and pH-responsive disassembly [51–56]. ProDs with different microRNA (miRNA) recognition capabilities can be simply prepared by altering the modules of DNAzyme and the incorporated corresponding cofactors of metal ions. Mechanistic studies revealed that the protection of ProDs relies on the immobilization of interferential proteins to the metal-phenolic nanoshells *via* the multiple intermolecular interactions generated from the catechol or galloyl groups of the phenolic building blocks. The pH-responsive coordination network of the protective nanoshells can also impart intracellular acidic responsiveness and cofactors self-supplying to cleavage the specific sequences of the designed DNAzymes during the endocytic process [44,55–59]. The rapid and highly accurate biosensing performance of the ProDs was evaluated by monitoring two abnormal expression miRNAs in living cells independently or simultaneously. We anticipate that the strategy of encapsulating Dzm-machines within multifunctional metal-phenolic nanoshells can be further developed in early clinical diagnosis with low intrinsic interferences and extended to a wide range of DNA/RNA-based technologies.

Dzm-machines were prepared by the assembly of substrate strands (Sub_{Zn}-21 and Sub_{Cu}-200b, Table S1 in Supporting information) and DNAzymes (*e.g.*, Dzm_{Zn} and Dzm_{Cu}) on ~15 nm gold nanoparticles (AuNPs, Fig. S2 in Supporting information) *via* the Au-S bond. The substrate strands were modified with fluorescent molecules such as carboxyfluorescein (FAM) and Cyanine5 (Cy5), while the DNAzymes were inactivated by their locking strands (L_{Zn}-21 and L_{Cu}-200b, Table S1 and Fig. S1a). As a typical example, the Dzm_{Zn}-machine remains inactivated in the absence of target strands 21 (T_{Zn}-21) because of the hybridization between Dzm_{Zn} and L_{Zn}-21. Meanwhile, fluorescence was quenched by the adjoining AuNPs (Fig. S1a).

We constructed a series of protected Dzm-machines ($ProD_{Zn}$, $ProD_{Cu}$, and $ProD_{Zn/Cu}$) by means of a biocompatible, polyphenol-based assembly method, which were equipped with various metal-phenolic nanoshells to protect the Dzm-machines from the interference caused by nucleases (*e.g.*, DNase I) and interfering proteins (*e.g.*, SSB protein) (Figs. S1b, c and e). ProDs can be internalized by cells with high efficiency (Fig. S1d), followed by the disassembly of metal-phenolic nanoshells in the acidic cytoplasm of living cells. Dzm-machine can be delivered in the cytosol and activated with the presence of the self-supplying cofactors (*i.e.*, Zn^{2+}, Cu^{2+}) to monitor the presence of targeted miRNAs in the cells (Fig. S1d).

The formation of metal-phenolic nanoshells can be confirmed by UV–vis absorption spectrophotometry and dynamic light scattering (DLS). Compared with AuNPs, the Dzm-machine presented a 5 nm red-shift in UV–vis spectra due to localized surface plasma resonance (520-525 nm) and exhibited a more negative zeta-potential (Fig. 1a and Fig. S3a in Supporting information). Negligible changes were observed on the nanoparticle size by transmission electron microscopy (TEM) (Fig. S3b in Supporting information). UV–vis spectra of ProD suspensions showed no obvious shift at 525 nm after nanoshell wrapping around the Dzm-machine, which indicated the formed nanoparticles remained monodispersed (Fig. S4a in Supporting information). As illustrated by the TEM images (Fig. 1b), ProDs incorporating different metal ions were further assembled to form uniform spherical nanoparticles with diameters of approximately 25 nm (Fig. S4b in Supporting information), in which the nanoshell was about 5 nm (Fig. S5 in Supporting information). In addition, ProDs showed more negative zeta-potential ($\xi = -40$ mV), which also suggested the successful assembly of nanoshell on the Dzm-machine (Fig. S6a in Supporting information) [37]. Furthermore, X-ray photoelectron spectroscopy (XPS) survey scan spectra confirmed the nanoshells wrapped on the surface of the Dzm-machine. As shown in Figs. S6b and c (Supporting information), compared with Dzm-machine, the Zn 2p peaks at 1021.8 eV and 1044.8 eV, the Cu 2p peaks at 932.6 eV and 952.2 eV were observed in survey scan spectra of $ProD_{Zn}$ and $ProD_{Cu}$, respectively, and they were simultaneously observed in survey scan spectra of $ProD_{Zn/Cu}$.

The pH-dependent assembly-disassembly kinetics of the nanoshells prepared with Zn^{II}-TA and Cu^{II}-TA were examined. Nanoshells disassembled rapidly at pH 5.5 compared with that at pH 7.4 (Fig. 1c and Fig. S7 in Supporting information). At pH 5.5, nanoshells (Zn^{II}-TA and Cu^{II}-TA) disassembled within 6 h, releasing more than 75% and 65% of Zn^{2+} and Cu^{2+}, respectively, due to the dissociation of coordination bonds between metal ions and phenolic groups. These results indicated that the acidic stimulation accelerated the release of Dzm-machines and metal ions from ProDs. In addition, the mechanisms of responsiveness and assembly process of target-initiated Dzm-machines were investigated by verified catalytic reactions of Dzm_{Zn} and Dzm_{Cu} *via* gel electrophoresis. We used target strand 21 (T_{Zn}-21, Table S1) and Dzm_{Zn} to evaluate the strand displacement reaction of L_{Zn}-21. As shown in Fig. 1d, in lane 6, the presence of a strong band corresponding to the hybrid of L_{Zn}-21 with the T_{Zn}-21 and the absence of the band of the single-stranded target sequence (T_{Zn}-21) further supported that the use of T_{Zn}-21 allowed for the complete displacement of the Dzm_{Zn} by the T_{Zn}-21. The Gibbs free energy (ΔG) of hybridization of L_{Zn}-21 with the Dzm_{Zn} was estimated as –23.99 kcal/mol (Fig. S8 in Supporting information), whereas the ΔG value of hybridization of T_{Zn}-21 with L_{Zn}-21 was –27.10 kcal/mol. Thus, the ΔG value of hybridization of T_{Zn}-21 with L_{Zn}-21 was smaller than that of L_{Zn}-21 with Dzm_{Zn}, which confirmed the preference of the strand displacement reaction by T_{Zn}-21.

The performance of the designed Dzm_{Zn} or Dzm_{Cu} highly depends on the cofactors Zn^{2+} or Cu^{2+} ions. As shown in Fig. S9a (Supporting information), the group Dzm_{Zn}/Sub_{Zn}-21 + Zn^{2+} was slightly lower than that of the group Dzm_{Zn}/Sub_{Zn}-21 in the gel images, which indicated that Dzm_{Zn} could effectively shear Sub_{Zn}-21 under the situation of Zn^{2+}. We confirmed other metal ions such as Ca^{2+} (1 mmol/L), Fe^{3+} (1 mmol/L), K^{+} (1 mmol/L), Mg^{2+} (1 mmol/L), and Mn^{2+} (0.1 mmol/L), showed a little effect to fuel Dzm_{Zn} and Dzm_{Cu} to cleave Sub_{Zn}-21 and Sub_{Cu}-200b at physiological condition

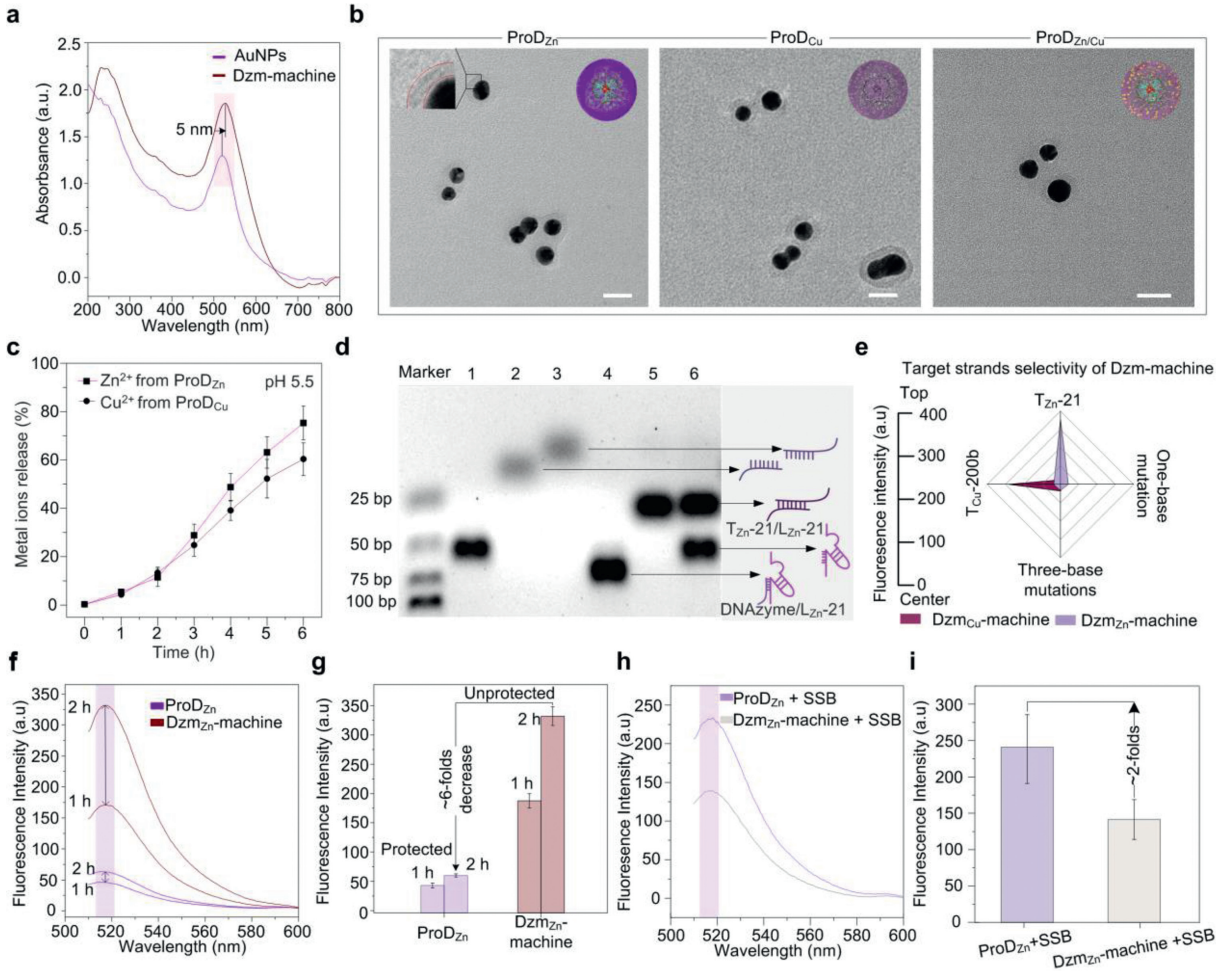

Fig. 1. Characterizations, designed recognization of single-stranded target sequences, and interference protection of ProDs. (a) UV–vis absorption spectra of AuNPs and Dzm-machine. (b) TEM images of different types of ProDs. Scale bars: 20 nm. (c) Zn^{2+} and Cu^{2+} release ratios of ProD$_{Zn}$ and ProD$_{Cu}$ at pH 5.5. (d) Gel images showed strand displacement of the Dzm$_{Zn}$ strands by the target strand (T$_{Zn}$-21), forming a duplex between the target and the locking strands (L$_{Zn}$-21). Lane 1, Dzm$_{Zn}$; Lane 2, L$_{Zn}$-21; Lane 3, T$_{Zn}$-21; Lane 4, the mixture of Dzm$_{Zn}$ and L$_{Zn}$-21; Lane 5, the mixture of L$_{Zn}$-21 and T$_{Zn}$-21; Lane 6, the mixture of Dzm$_{Zn}$/L$_{Zn}$-21 duplex and T$_{Zn}$-21. (e) Radar plot analysis of the fluorescence signal of the Dzm$_{Zn}$-machine (Dzm$_{Cu}$-machine) initiated by T$_{Zn}$-21 (T$_{Cu}$-200b), one base mutation, three base mutations, or T$_{Cu}$-200b (T$_{Zn}$-21) in the presence. Error bars showed the standard deviations of three independent experiments. (f, g) Fluorescence analysis after ProD$_{Zn}$ and Dzm$_{Zn}$-machine incubated in solutions containing 5 U/mL of DNase I at different time. (h, i) Fluorescence analysis of ProD$_{Zn}$ and Dzm$_{Zn}$-machine detecting T$_{Zn}$-21 after incubation in 10 μg/mL SSB protein solutions.

(green fluorescence of FAM and red fluorescence of Cy5), where Dzm$_{Zn}$ and Dzm$_{Cu}$ were assembled on AuNPs without the locking strands (Fig. S9b in Supporting information) [60]. Next, the specificity of the Dzm$_{Zn}$-machine (Dzm$_{Cu}$-machine) was analyzed by testing two variants of T$_{Zn}$-21 (T$_{Cu}$-200b) and T$_{Cu}$-200b (T$_{Zn}$-21). These two variants were designed to have single-base or three-base mutations (Table S1). As shown in Fig. 1e, the T$_{Zn}$-21-induced fluorescence increase was more significant than that induced by two variants and T$_{Cu}$-200b at the same concentration. The high degree miRNA-specific recognition of the Dzm-machine could be attributed to the usage of the locking strand.

Functional DNA materials have been applied in diverse biological systems. However, the challenge has always stemmed from extrinsic interferences leading to arising of false-positive signals. DNase I, a common endonuclease, is capable of effectively degrading both single- and double-stranded DNA. SSB protein is a protein that bonds with single-stranded DNA to prevent repairing and forming double-stranded DNA or being degraded by nucleases. Therefore, to demonstrate the ability of nanoshell to address this challenge, the interactions of ProD$_{Zn}$ with DNase I and SSB protein were investigated. Nanoshell-protected ProD$_{Zn}$ and native Dzm$_{Zn}$-machine were both treated with 0.05 U/mL of DNase I and 5 U/mL of DNase I, respectively (Fig. S10a in Supporting information). When treated with a lower concentration of DNase I (0.05 U/mL) up to 6 h, no obvious changes were observed with the fluorescence intensity of FAM modifying on Sub-21 (Fig. S11 in Supporting information), which confirmed that even native Dzm$_{Zn}$-machine could enhance the nuclease resistance of the oligonucleotides. However, when the two samples were treated with a higher concentration of DNase I (5 U/mL) for 2 h, as shown in Figs. 1f and g, a significant increase of the FAM fluorescence intensity was observed in the Dzm$_{Zn}$-machine, which leads to the false-positive signals arisen from the high concentration of nuclease solution. In contrast, ProD$_{Zn}$ was still stable in 5 U/mL of DNase I solution. ProD$_{Zn}$ possessed stability towards nuclease hydrolysis with 6-folds over Dzm$_{Zn}$-machine.

In addition, the effects of SSB protein binding were also studied by monitoring the changes of the fluorescence intensity of FAM, which ProD$_{Zn}$ and Dzm$_{Zn}$-machine were used to detect T$_{Zn}$-21, respectively (Fig. S10b in Supporting information). As shown in Figs. 1h and i, Sub$_{Zn}$-21 from Dzm$_{Zn}$-machine without the protection from the nanoshell was obstructed by SSB protein and could not be

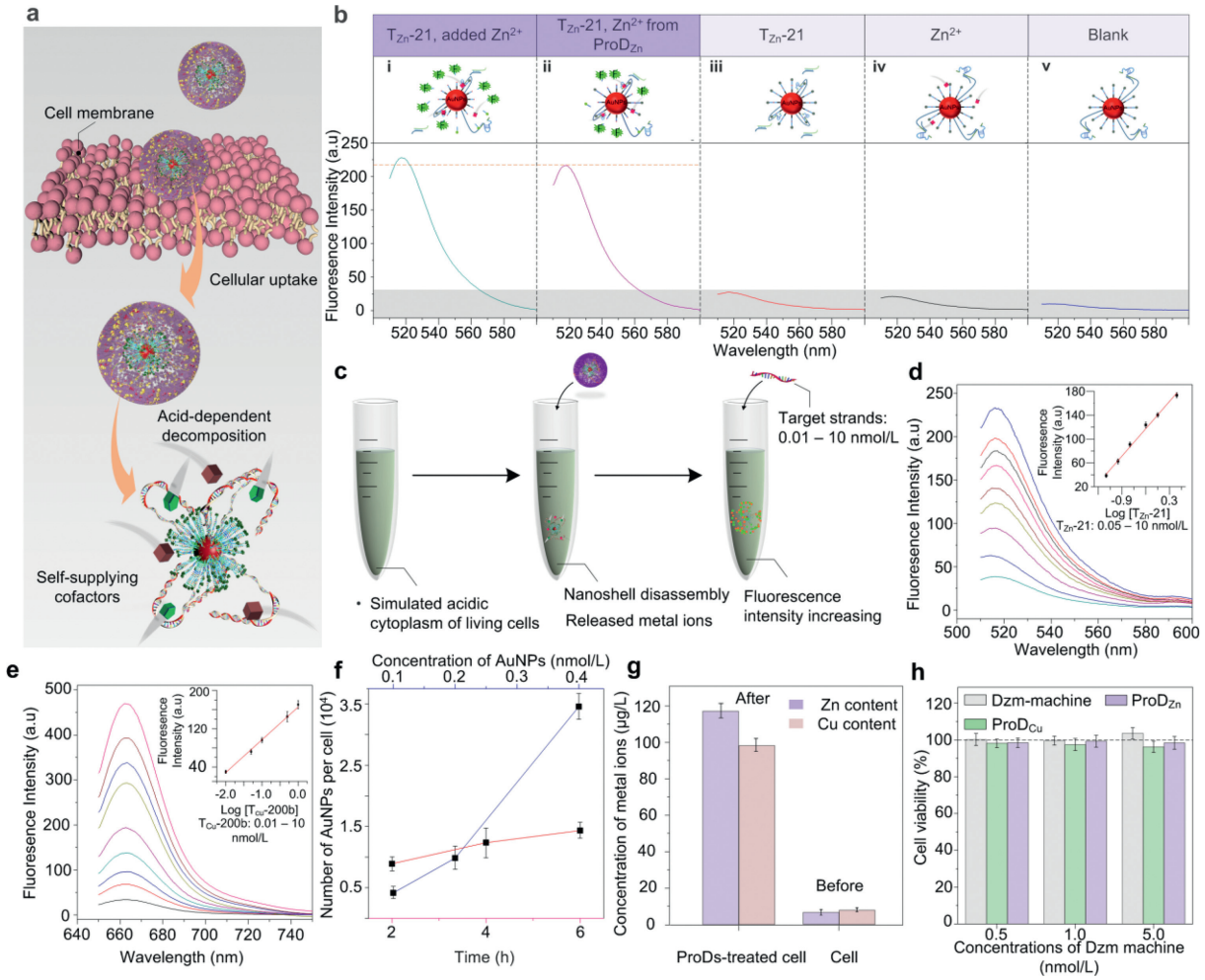

Fig. 2. ProDs activation in the simulated acidic cytoplasm and cellular uptake. (a) Schematic of the ProD cellular uptake and the acid responsiveness. (b) Activation of Dzm_{Zn}-machine by Zn^{2+} and T_{Zn}-21. (c) Schematic of the detection target strands of different concentrations by $ProD_{Zn}$ and $ProD_{Cu}$. Fluorescence spectra of (d) T_{Zn}-21 and (e) T_{Cu}-200b with concentration ranges of 0.05–10 nmol/L and 0.01–10 nmol/L. Insets: plot of increased fluorescence intensity *versus* the target strand concentrations. (f) ICP-MS analysis of the number of AuNPs in Hela cells after Hela cells treatment with ProDs at different concentrations and times. (g) ICP-MS analysis of Zn and Cu content in Hela cells before and after 0.1 nmol/L of $ProD_{Zn}$ and $ProD_{Cu}$ treatments. (h) The cell viability of Hela cells that were incubated with different concentrations of Dzm-machine, $ProD_{Zn}$, and $ProD_{Cu}$. Error bars showed the standard deviations of three independent experiments.

efficiently cleaved by Dzm_{Zn}. However, $ProD_{Zn}$ only showed a negligible effect by SSB protein, which was indicated by the 2 times higher fluorescence intensity of $ProD_{Zn}$ than that of the Dzm_{Zn}-machine. These results demonstrated that $ProD_{Zn}$ was more stable than the Dzm_{Zn}-machine in the presence of SSB protein.

To further investigate the protective mechanism of the nanoshell to the Dzm-machine, we synthesized a free-standing nanoshell without the presence of the Dzm_{Zn}-machine (observed as hollow structured nanoshells). These nanoshells were added to the solutions containing 10 μg/mL of human serum albumin labeled with fluorescein isothiocyanate isomer (HAS-FITC). By analyzing the internal fluorescence intensity of nanoshells, we can measure the percentage of impermeable nanoshells to indicate the protective effect of nanoshells. Our results suggested that the protected efficiency of the nanoshell showed no changes through the 1 h incubation (Figs. S10c and d in Supporting information). Previous works on the metal-phenolic-based materials have shown that the average pore sizes of the mesh-like network were large enough for 200 kDa molecules to pass through (Molecule weights of DNase I, SSB protein, and HSA are 32, 74 and 66 kDa, respectively.) [32]. Therefore, we further investigated the reason why the HSA cannot pass through the shells. The fluorescence proteins were found to remain on the nanoshells after being washed 3 times or disassembled, which indicated that the nanoshell could protect the internal Dzm-machine due to the adsorption of proteins on the protective shells *via* intermolecular interactions between proteins and the polyphenol moieties in the nanoshells (Fig. S10e in Supporting information). miRNAs play critical roles in many biological processes and are vital biomarkers for disease diagnostics. It is of significance to develop miRNA biosensors with fast responses, high sensitivity, and excellent reliability in living cells. Previous works have demonstrated that the DNAzyme-based SNAs were designed to detect the biomarkers in living cells. However, the metal ions of the DNAzyme cofactor need to be added into the culture solution to activate the DNAzymes [10,25,36,61]. Therefore, we studied the cellular internalization of ProDs and their self-catalytic detection of targeted miRNAs (Fig. 2a). Dzm_{Zn}-machine was activated and exhibited a strong fluorescence signal in the presence of 0.1 mmol/L Zn^{2+} and 100 nmol/L miRNA 21 (Fig. 2b (i)). Whereas the Dzm_{Zn}-machine was inactivated in the absence of T_{Zn}-21 or Zn^{2+} and the fluorescence intensity significantly decreased (Fig. 2b (iii, iv)). Meanwhile, the disassembled nanoshell layer (Zn^{II}-TA) was added to the Dzm_{Zn}-machine solution containing 100 nmol/L T_{Zn}-21, and then Dzm_{Zn}-machine was activated. The fluorescence intensity

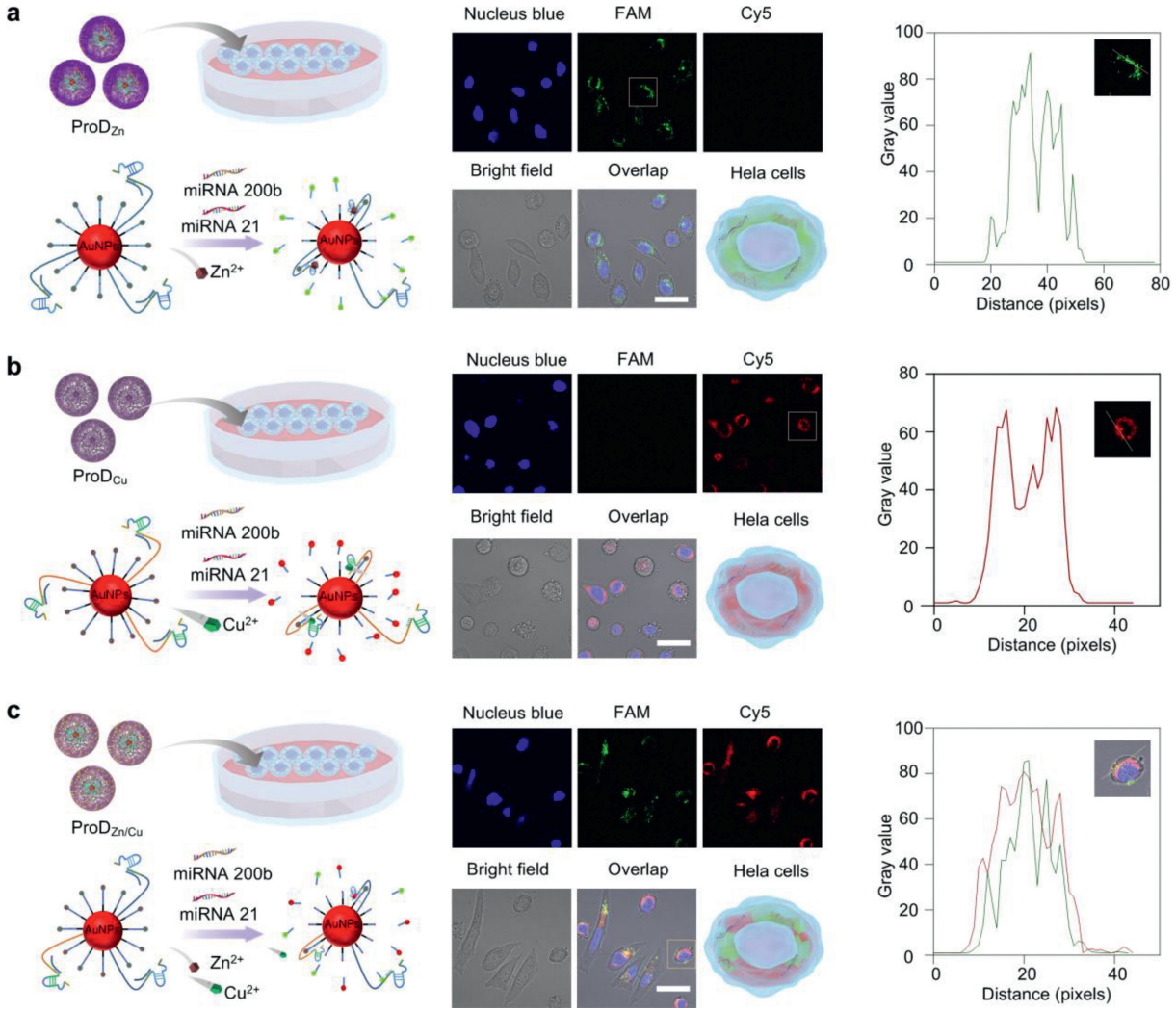

Fig. 3. Biosensing performance of ProDs on the intracellular imaging of targeted miRNAs. Fluorescence images of detecting miRNA 21 and miRNA 200b in Hela cells by (a) ProD$_{Zn}$, (b) ProD$_{Cu}$ and (c) ProD$_{Zn/Cu}$. The fluorescence intensity analysis was performed by ImageJ. The concentration of ProDs was 1 nmol/L. Scale bars: 20 μm.

(Fig. 2b (ii)) showed no difference from that in Fig. 2b (i). The results further confirmed ProDs could spontaneously self-supply the requisite metal ions for DNAzyme to cleave substrate strands.

We evaluated the fluorescence increases of ProD$_{Zn}$ and ProD$_{Cu}$ induced by different concentrations of T$_{Zn}$-21 and target strand 200b (T$_{Cu}$-200b), respectively, in the simulated acidic cytoplasm of living cells. As shown in Fig. 2c, nanoshell could disassemble in an acidic solution (pH 5.5) to release specific metal ions and Dzm-machines. The fluorescence intensity was found to increase with the increase of T$_{Zn}$-21 and T$_{Cu}$-200b concentrations. The concentration ranges of T$_{Zn}$-21 and T$_{Cu}$-200b were 0.05–10 nmol/L and 0.01–10 nmol/L, respectively, and the inset of Figs. 2d and e showed linear correlations between fluorescence intensity and log [target strand] ($R^2_{ProDZn} = 0.9943$ and $R^2_{ProDCu} = 0.9954$) with the limit of detection (LOD) of 5.4 pmol/L and 0.98 pmol/L, based on the 3σ/slope rule.

To evaluate the cellular uptake efficiencies of the ProDs, Hela cells were treated with ProD$_{Zn}$ and ProD$_{Cu}$ for 6 h and the concentrations of Au inside cells were measured. Inductively coupled plasma mass spectrometry (ICP-MS) measurements showed that the content of Au increases with the increase of both the ProDs concentration and time of incubation (Fig. 2f). The number of ProDs showed no obvious decrease inside cells compared to Dzm-machine (Fig. S12 in Supporting information). In addition, the concentration of Zn^{2+} and Cu^{2+} in the cells after ProDs (ProD$_{Zn}$ and ProD$_{Cu}$) treatment also increased from 5.59 and 6.33 μg/L to 117.2 and 96.36 μg/L, respectively (Fig. 2g). Collectively, ProDs possessed a highly efficient cellular uptake, and the released Zn^{2+} and Cu^{2+} ions in the cytoplasm were sufficient for the activation of Dzm-machines.

To investigate the cytotoxicity of the ProDs, Cell Counting Kit-8 (CCK-8) assay was performed on Hela cells. ProDs with differently designed cofactors of metal ions were co-incubated with Hela cells for 24 h. The cell viability remained over 96% when the concentration of Dzm-machine and ProDs reached up to 5 nmol/L (Fig. 2h). Moreover, after being incubated with the Dzm-machine and ProDs, the Hela cells were stained with Calcein-AM/Propidium Iodide (PI) cell viability assay kit, followed by intracellular imaging using optical image microscopy, which supported the results of the CCK-8 assay (Fig. S13 in Supporting information). Flow cytometry further confirmed the low toxicity of ProDs to living cells (Fig. S14 in Supporting information).

We further investigated the ability of ProDs to monitor specific miRNAs in living cells. Hela cells, with high miRNA 21 and miRNA 200b expression profiles, were chosen as the model cells to evaluate the feasibility of ProDs for *in situ* visualizations of intracellular targeted miRNAs [62]. Confocal microscopy images show that ProD$_{Cu}$ could continuously monitor miRNA 200b in Hela cells

and the Cy5 signal (red fluorescence) increased with an incubation time up to 6 h (Fig. S15 in Supporting information). Therefore, Hela cells were treated with ProDs for 6 h in the subsequent experiments. Hela cells presented obvious green fluorescence from FAM after being treated with $ProD_{Zn}$ and presented obvious red fluorescence from Cy5 after being treated with $ProD_{Cu}$ (Figs. 3a and b). These results indicated that $ProD_{Zn}$ and $ProD_{Cu}$ could provide self-sufficient cofactors of intracellular Zn^{2+} and Cu^{2+} ions in the Hela cells (without the external addition of cofactors) and could recognize miRNA 21 and miRNA 200b to generate fluorescent signals, respectively.

Some significant cellular processes are regulated by multiple miRNAs collaboratively and simultaneously, especially in some cancer cells. Therefore, the precise imaging of multiple miRNAs expression in living cells is of great significance in clinical diagnosis. Confocal microscopy images demonstrated that $ProD_{Zn/Cu}$ could simultaneously monitor miRNA 21 and miRNA 200b in Hela cells, as observing green fluorescence signals from FAM and red fluorescence signals from Cy5 (Fig. 3c), which was derived from the system-specific self-providing different cofactors for different Dzm probes.

Furthermore, to test the specificity of $ProD_{Zn/Cu}$ for multiple miRNAs in living cells, human renal epithelial cells (293T), human breast cancer MCF-7 cells (Overexpress miRNA 21), and human cervical cancer Hela cells (Overexpress miRNA 21 and miRNA 200b) were chosen to image the levels of miRNA 21 and miRNA 200b. With the confocal image analysis (Fig. S16 in Supporting information), Hela cells showed obvious green fluorescence signals (FAM) and red fluorescence signals (Cy5). However, MCF-7 cells only displayed obvious green fluorescence signals (FAM). In addition, no obvious fluorescence signals were produced due to the low expression of miRNA 21 and miRNA 200b in 293T cells. The results further confirmed that ProDs designed with a multiple cofactor mechanism have a high sensitivity and accuracy to monitor multiple miRNAs in living cells.

In this work, we constructed a series of ProDs with different cofactor designs, including $ProD_{Zn}$, $ProD_{Cu}$ and $ProD_{Zn/Cu}$, through the encapsulation of Dzm-machines within the metal-phenolic nanoshells. The nanoshells showed the ability to protect the Dzm-machines from the interference of DNase I and SSB proteins to avoid false-positive signals. This protection is derived from the interfacial inactivation of the interferential proteins *via* the multiple intermolecular interactions between phenolic moieties and proteins. Furthermore, the formation of nanoshells facilitated the cellular internalization of ProDs. The disassembly of nanoshells concomitantly released metal ions intracellularly, acting as self-supplying cofactors to fuel the biocatalytic operation of different Dzm-machines. Meanwhile, ProDs presented the specificity and sensitivity in monitoring multiple tumor-related miRNAs in living cells simultaneously. The ProDs can be expanded to recognize multiple disease-related miRNAs by altering the modules of the Dzm sequence in the functional core and the chelated metal ions in the protective nanoshells. Our work not only presents a facile and rapid strategy for engineered Dzm-machines to overcome the shortcomings in practical applications, but also contributes to a conceptual and practical paradigm for effective protection of DNA/RNA-based materials in a wide range of applications, such as a vaccine, therapy, and information storage.

Declaration of competing interest

The authors declare that they have no known competing financial interests or personal relationships that could have appeared to influence the work reported in this paper.

Acknowledgments

This work was supported by National Talents Program, Double First Class University Plan of Sichuan University, State Key Laboratory of Polymer Materials Engineering (No. sklpme 2020-03-01), Natural Science Foundation of Sichuan Province (Nos. 2022NSFSC1735, 2023NSFSC1097), Fundamental Research Funds for the Central Universities (No. ZYN2022094), National Natural Science Foundation of China (Nos. 22178233, 22208228), China Postdoctoral Science Foundation (No. 2020TQ0209), Fundamental Research Funds for the Central Universities (No. YJ201959), Science and Technology Support Program of Sichuan Province (No. 2021YJ0414) and Project of Chengdu Science and Technology Bureau (No. 2021-YF05-02110-SN).

Supplementary materials

Supplementary material associated with this article can be found, in the online version, at doi:10.1016/j.cclet.2023.108200.

References

[1] T. Zhang, T. Tian, Y. Lin, Adv. Mater. 34 (2022) 2107820.
[2] M. Madsen, K.V. Gothelf, Chem. Rev. 119 (2019) 6384–6458.
[3] M. Xiao, W. Lai, T. Man, et al., Chem. Rev. 119 (2019) 11631–11717.
[4] S. Khan, B. Burciu, C. Filipe, et al., ACS Nano 15 (2021) 13943–13969.
[5] A. Chakraborty, S.P. Ravi, Y. Shamiya, C. Cui, A. Paul, Chem. Soc. Rev. 50 (2021) 7779–7819.
[6] L. Liu, F. Hong, H. Liu, et al., Sci. Adv. 8 (2022) eabm9530.
[7] L. He, D. Lu, H. Liang, et al., ACS Nano 11 (2017) 4060–4066.
[8] S. Li, L. Xu, W. Ma, et al., J. Am. Chem. Soc. 138 (2016) 306–312.
[9] J. Wei, H. Wang, Q. Wu, et al., Angew. Chem. Int. Ed. 59 (2020) 5965–5971.
[10] W. Wang, N. Satyavolu, Z. Wu, et al., Angew. Chem. Int. Ed. 56 (2017) 6798–6802.
[11] Y. Li, K. Liu, B. Wang, et al., J. Hazard. Mater. 440 (2022) 129712.
[12] L. Zhou, A. Chandrasekaran, J. Punnoose, et al., Sci. Adv. 6 (2020) eabc6246.
[13] Y. Dong, C. Yao, Y. Zhu, D. Luo, D. Yang, Chem. Rev. 120 (2020) 9420–9481.
[14] Z. Wang, J. Yang, G. Qin, et al., Angew. Chem. Int. Ed. 61 (2022) e202204291.
[15] H. Wang, Y. Chen, H. Wang, et al., Angew. Chem. Int. Ed. 58 (2019) 7380–7384.
[16] F. Li, Y. Liu, Y. Dong, et al., J. Am. Chem. Soc. 144 (2022) 4667–4677.
[17] F. Li, N. Song, Y. Dong, et al., Angew. Chem. Int. Ed. 61 (2021) e202116569.
[18] J. Dong, Y. Ouyang, J. Wang, M. O'Hagan, I. Willner, ACS Nano 16 (2022) 6153–6164.
[19] Y. Zhao, R. Li, J. Sun, et al., ACS Nano 16 (2022) 5404–5417.
[20] H. Zhao, Z. Zhang, D. Zuo, et al., Nano Lett. 21 (2021) 5377–5385.
[21] R. Breaker, G. Joyce, Chem. Biol. 1 (1994) 223–229.
[22] W. Zhou, R. Saran, J. Liu, Chem. Rev. 117 (2017) 8272–8325.
[23] Y. Wang, K. Nguyen, R. Spitale, J. Chaput, Nat. Chem. 13 (2021) 319–326.
[24] J. Borggräfe, J. Victor, H. Rosenbach, et al., Nature 601 (2022) 144–149.
[25] Y. Zhang, X. Zhang, Y. Li, et al., Chem. Sci. 11 (2020) 6289–6296.
[26] M. Xiong, Z. Yang, J. Li, et al., Angew. Chem. Int. Ed. 59 (2020) 1891–1896.
[27] R. Lake, Z. Yang, J. Zhang, Y. Lu, Acc. Chem. Res. 52 (2019) 3275–3286.
[28] Y. Xiong, J. Zhang, Z. Yang, et al., J. Am. Chem. Soc. 142 (2020) 207–213.
[29] H. Vaughan, J. Green, S. Tzeng, Adv. Mater. 32 (2020) e1901081.
[30] J. Cutler, E. Auyeung, C. Mirkin, J. Am. Chem. Soc. 134 (2012) 1376–1391.
[31] H. Fan, X. Zhang, Y. Lu, Sci. China Chem. 60 (2017) 591–601.
[32] X. Fu, G. Ke, F. Peng, et al., Nat. Commun. 11 (2020) 1518.
[33] L. Shi, W. Wu, Y. Duan, et al., ACS Nano 15 (2021) 1841–1849.
[34] H. Liu, X. Yu, Y. Chen, et al., Nat. Commun. 8 (2017) 2006.
[35] J. Wang, L. Yue, Z. Li, et al., Nat. Commun. 10 (2019) 4963.
[36] H. Peng, X. Li, H. Zhang, X.C. Le, Nat. Commun. 8 (2017) 14378.
[37] C. Jung, P. Allen, A. Ellington, Nat. Nanotechnol. 11 (2016) 157–163.
[38] D. Samanta, S. Ebrahimi, C. Kusmierz, H. Cheng, C. Mirkin, J. Am. Chem. Soc. 142 (2020) 13350–13355.
[39] D. Seferos, A. Prigodich, D. Giljohann, P. Patel, C. Mirkin, Nano Lett. 9 (2009) 308–311.
[40] S. Peng, B. Bie, Y. Sun, et al., Nat. Commun. 9 (2018) 1293.
[41] K. Su, S. Du, W. Wang, D. Yuan, Chin. Chem. Lett. 31 (2020) 2023–2026.
[42] C. Shi, L. Li, L. Yang, Y. Li, Chin. Chem. Lett. 31 (2020) 1951–1955.
[43] X. Meng, K. Zhang, W. Dai, et al., Chem. Sci. 9 (2018) 7419–7425.
[44] J. Guo, M. Suástegui, K.K. Sakimoto, et al., Science 362 (2018) 813–816.
[45] J. Guo, B.L. Tardy, A.J. Christofferson, et al., Nat. Nanotechnol. 11 (2016) 1105–1111.
[46] J. Guo, Y. Ping, H. Ejima, et al., Angew. Chem. Int. Ed. 53 (2014) 5546–5551.
[47] H. Geng, Q. Zhong, J. Li, et al., Chem. Rev. 122 (2022) 11432–11473.
[48] J. Pan, G. Gong, Q. Wang, et al., Nat. Commun. 13 (2022) 2117.
[49] Z. Zhao, D. Pan, Q. Qi, et al., Adv. Mater. 32 (2020) 2003492.
[50] K. Li, G. Xiao, J.J. Richardson, et al., Adv. Sci. 6 (2019) 1801688.
[51] X. Qiu, X. Wang, Y. He, et al., Sci. Adv. 7 (2021) eabh3482.

[52] Y. Ju, H. Liao, J.J. Richardson, J. Guo, F. Caruso, Chem. Soc. Rev. 51 (2022) 4287–4336.
[53] Q. Dai, H. Geng, Q. Yun, J. Hao, J. Cui, Theranostics 9 (2019) 3170–3190.
[54] Q. Wang, Z. Gao, K. Zhao, et al., Chin. Chem. Lett. 33 (2022) 1917–1922.
[55] H. Ejima, J.J. Richardson, K. Liang, et al., Science 341 (2013) 154–157.
[56] Q. Wang, Z. Gao, Q. Zhong, et al., Langmuir 37 (2022) 11292–11300.
[57] P. Pan, X. Chen, H. Xing, et al., Chin. Chem. Lett. 32 (2021) 2159–2163.
[58] H. Wang, C. Wang, Y. Zou, et al., Giant 3 (2020) 100022.
[59] J. Chen, J. Li, J. Zhou, et al., ACS Nano 13 (2019) 11653–11664.
[60] W. Moon, P. Huang, J. Liu, Biochemistry 60 (2021) 1909–1918.
[61] K. Chen, Q. Huang, T. Fu, et al., Anal. Chem. 92 (2020) 7404–7408.
[62] A. Qu, M. Sun, L. Xu, et al., Proc. Natl. Acad. Sci. U. S. A. 116 (2019) 3391–3400.